Development of a Hydroplane Prediction Tool (Final Report)

FDOT Contract No. & Task Work Order (BDK82 977-08)

Submitted by

N. Mike Jackson, Ph.D., P.E.
Principal Investigator
University of North Florida
School of Engineering
One UNF Drive
Jacksonville, FL 32224-2645
Phone : (904) 620-1847
Email: njackson@unf.edu

and

Paul J. Sander
Research Assistant
University of North Florida
One UNF Drive
Jacksonville, FL 32224-2645

Submitted to

The Florida Department of Transportation
Research Center
605 Suwannee Street, MS 30
Tallahassee, FL 32399

July 31, 2013

DISCLAIMER

The opinions, findings, and conclusions expressed in this publication are those of the authors and not necessarily those of the State of Florida Department of Transportation.

SI CONVERSION FACTORS

APPROXIMATE CONVERSIONS TO SI UNITS USED

SYMBOL	WHEN YOU KNOW	MULTIPLY BY	TO FIND	SYMBOL
LENGTH				
in	Inches	25.4	millimeters	mm
ft	Feet	0.305	meters	m
yd	Yards	0.914	meters	m

SYMBOL	WHEN YOU KNOW	MULTIPLY BY	TO FIND	SYMBOL
AREA				
in^2	Square inches	645.2	square millimeters	mm^2
ft^2	Square feet	0.093	square meters	m^2
yd^2	square yard	0.836	square meters	m^2

SYMBOL	WHEN YOU KNOW	MULTIPLY BY	TO FIND	SYMBOL
VOLUME				
ft^3	cubic feet	0.028	cubic meters	m^3
yd^3	cubic yards	0.765	cubic meters	m^3
NOTE: volumes greater than 1000 L shall be shown in m^3				

SYMBOL	WHEN YOU KNOW	MULTIPLY BY	TO FIND	SYMBOL
MASS				
oz	ounces	28.35	grams	g
lb	pounds	0.454	kilograms	kg

SYMBOL	WHEN YOU KNOW	MULTIPLY BY	TO FIND	SYMBOL
FORCE and PRESSURE or STRESS				
lbf	Pound force	4.45	Newton	N
lbf/in^2	Pound force per square inch	6.89	kilopascals	kPa

Technical Report Documentation Page

1. Report No.	2. Government Accession No.	3. Recipient's Catalog No.
4. Title and Subtitle Development of a Hydroplane Prediction Tool		5. Report Date July, 2013
		6. Performing Organization Code
7. Author(s) N. Mike Jackson and Paul Sander		8. Performing Organization Report No.
9. Performing Organization Name and Address University of North Florida One UNF Drive Jacksonville, FL 32224		10. Work Unit No. (TRAIS)
		11. Contract or Grant No. BDK82 977-08
12. Sponsoring Agency Name and Address Florida Department of Transportation 605 Suwannee St. MS 30 Tallahassee, Florida 32399 (850)414-4615		13. Type of Report and Period Covered Final Report April, 2012 – July, 2013
		14. Sponsoring Agency Code
15. Supplementary Notes		

16. Abstract

Researchers have long known that there is a relationship between wet-weather crash rate and pavement friction. It is also well known that increasing speed and water film thickness (WFT) increases the likelihood of hydroplaning. Hydroplaning refers to the separation of the tire contact from the pavement surface by a layer of water. This is a complex phenomenon that is affected by the WFT on the pavement surface, pavement macro-texture, tire tread depth, tire inflation pressure, tire contact area, and vehicle speed. In recognition of this, the Florida Department of Transportation (FDOT) State Materials Office (SMO) routinely monitors pavement surface macro-texture, friction, and other pavement-related properties for the empirical assessment of hydroplaning potential.

The objective of this research was to develop a methodology for the reliable prediction of hydroplaning speed for specific pavement design surfaces and materials employed on Florida roadways. The research consisted of modeling of hydroplaning conditions on typical FDOT roadway sections. This modeling was based on pavement condition inputs as obtained from field surveys currently performed by FDOT.

A mechanistic/empirical prediction tool was developed based on the research conducted. The proposed prediction tool has been transferred to the FDOT for further evaluation and practical use.

17. Key Word	18. Distribution Statement
Hydroplane, Prediction, Empirical, Friction, Texture, Speed, Driver Safety.	No Restrictions

19. Security Classif. (of this report)	20. Security Classif. (of this page)	21. No. of Pages	22. Price
Unclassified	Unclassified	27	

Form DOT F 1700.7 (8-72) Reproduction of completed page authorized

EXECUTIVE SUMMARY

Researchers have long known that there is a relationship between wet-weather crash rate and pavement friction. It is also well known that increasing speed and water film thickness (WFT) increases the likelihood of hydroplaning. Hydroplaning refers to the separation of the tire contact from the pavement surface by a layer of water. This is a complex phenomenon that is affected by the WFT on the pavement surface, pavement macro-texture, tire tread depth, tire inflation pressure, tire contact area, and vehicle speed. In recognition of this, the Florida Department of Transportation (FDOT) State Materials Office (SMO) routinely monitors pavement surface macro-texture, friction, and other pavement-related properties for the empirical assessment of hydroplaning potential.

The objective of this research was to develop a methodology for the reliable prediction of hydroplaning speed for specific pavement design surfaces and materials employed on Florida roadways. The research consisted primarily of an extensive literature review and modeling effort.

The resulting mechanistic/empirical model is based on the literature and observed pavement condition inputs as obtained from field surveys performed by FDOT. The final product, a proposed hydroplane prediction tool, is presented in a MS Excel format for ease of use, and has been provided to the FDOT for further evaluation and practical implementation.

Development of a Hydroplane Prediction Tool

CONTENTS

List of Figures vii
List of Tables ix
Literature Review 1
National Aeronautics and Space Administration 1
Northwestern University and General Motors Corporation 2
National University of Singapore 3
2D CFD Model 4
3D CFD Model 4
3D FSI Model 5
3D FSI Model for Friction Number Determination 7
3D Finite Element Model Development 9
Overall Concept of Model 9
Structural Modeling 9
Fluid Modeling 14
Empirical FN-Speed Model Development 16
Conclusions 16
References 16
Appendix 16

LIST OF FIGURES

Figure 1. A 6.50-13 Smooth Tread Tire Hydroplaning Above a Glass Plate. Vertical Load = 835 lb_f, Tire Pressure = 27 psi. Reproduced from Figure 2, Horne and Joyner, 1965 [3]..... 2

Figure 2. Schematic of Milled Aluminum Plate from Browne's PhD Experiment. Reproduced from Figure 3-1, Browne, 1971 [4]..... 3

Figure 3. Schematic of Ong's Two-Dimensional CFD Model. Reproduced from Figure 3.6, Ong, 2006 [6]..... 4

Figure 4. Schematic of Ong's Three-Dimensional CFD Model. Reproduced from Figure 3.5, Ong, 2006 [6]..... 5

Figure 5. Ong's Pneumatic Tire Sub-Model. Reproduced from Figure 7.1a, Ong, 2006 [6]..... 5

Figure 6. Ong's Fluid Sub-Model. Reproduced from Figure 7.1b, Ong, 2006 [6]..... 6

Figure 7. Comparison of Ong's Simulation Results with Experimental Data from Rose and Gallaway and Horne. Reproduced from Figure 8.1, Ong, 2006 [6]. 8

Figure 8. Comparison of Ong's Simulation Results with Experimental Data from Horne and Horne and Tanner. Reproduced from Figure 8.1, Ong, 2006 [6]. 8

Figure 9. Comparison of Ong's Simulation Results with Experimental Data from Horne and Tanner and Agrawal and Henry. Reproduced from Figure 8.1, Ong, 2006 [6]..... 8

Figure 10. Wheel Frame of Reference. Adapted from Figure 3.2, Ong, 2006 [6]..... 10

Figure 11. AutoCAD trace of Figure 2 from ASTM E 524 Standard Smooth Tire. 11

Figure 12. AutoCAD trace of Figure 2 from ASTM E 524 Standard Smooth Tire with center line. 12
Figure 13. ASTM E 524 Standard Smooth Tire cross section in ADINA..... 12

Figure 14. ASTM E 524 Standard Smooth Tire in ADINA. 13

Figure 15. Meshed ASTM E 524 Standard Smooth Tire and Planar Pavement Surface in ADINA. 14
Figure 16. Fluid Geometry with Boundary Conditions. 15

Figure 17. Fluid Mesh in ADINA..... 15

Figure 18. Friction Number and the Contributions from Fluid Drag and Tire-Pavement Contact. Reproduced from Figure 8.2a, Ong, 2006 [6]..... 16

Figure 19. Recreation of Figure 7 using the Total FN Curve from Figure 18. 17

Figure 20. Recreation of Figure 8 using the Total FN Curve from Figure 18. 17

Figure 21. Recreation of Figure 9 using the Total FN Curve from Figure 18. 18

Figure 22. Total FN Curve from Figure 18 Matched to Data from Younger, 1994 [21], [22] shown in Zhang, 2012 [20]. Left: Data for 50 mm Porous Layer Thickness. Right: Data for 100 mm Porous Layer Thickness. 19

Figure 23. Hydroplaning Curves Matched to the Data from Dense Graded Sites from Jackson et al., 2008 [23]. 19

Figure 24. Hydroplaning Curves Matched to the Data from Open Graded Sites from Jackson et al., 2008 [23]. 20

Figure 25. Hydroplaning Curves Matched to the Data from Dense Graded Sites from Choubane et al., 2012 [24]. 21

Figure 26. Hydroplaning Curves Matched to the Data from Open Graded Sites from Choubane et al., 2012 [24]. 22

Figure 27. Hydroplaning Curve for Site 3 from Jackson, 2008 [23]. 24

LIST OF TABLES

Table 1. Structural Components of the Standard Smooth Tire and Their Properties. 6

Table 2. Surface Type Contants. 23

Table 3. Aggregate Constants. 23

Table 4. Default Values of Speed and Friction Number. 23

Table 5. Values of Speed and FN for Site 3 from Jackson, 2008 [23]. 24

LITERATURE REVIEW

The study of hydroplaning phenomena has been active since the early 1960s. Although there are many authors and researchers associated with this field, this literature review will focus on a few key groups that have made significant advances in experimental and/or theoretical work related to hydroplaning.

National Aeronautics and Space Administration

Many researchers at NASA participated in the performance and evaluation of some of the earliest documented pneumatic tire hydroplaning experiments. In particular, Walter B. Horne, Robert C. Dreher and Trafford J. W. Leland are responsible for a significant portion of the hydroplaning research conducted at NASA. Several studies were performed for both automobile and aircraft tires.

In the report "Phenomena of Pneumatic Tire Hydroplaning," Horne and Dreher reveal what is now known as the NASA hydroplaning equation:

$$V_p = 10.35\sqrt{p}$$

where V_p is the hydroplaning speed in mph and p is the tire pressure in psi [1]. This equation is valid "for smooth and closed pattern tread tires which do not allow escape paths for water, and for rib tread tires on fluid covered runways where the fluid depth exceeds the groove depths in the tread of these tires" [1]. This equation was derived from work reported in an earlier report by Horne and Leland, "Influence of Tire Tread Pattern and Runway Surface Condition on Braking Friction and Rolling Resistance of a Modern Aircraft Tire" where the water depth was between 0 and 0.3 inches on concrete surfaces and between 0 and 0.5 inches on asphalt surfaces [2].

In the report "Pneumatic Tire Hydroplaning and Some Effects on Vehicle Performance," Horne and Joyner display the photographic results of a smooth tread automobile tire during different stages of hydroplaning [3]. As shown in Figure 1, the separation of the tire from the glass surface increases with increasing speed. This agrees with the theory that the likelihood of hydroplaning increases with increasing speed where all conditions other than speed are held constant.

Although NASA hydroplaning research continued at least until the late 1970s, much of the early work is fundamental to the field of hydroplaning. Dozens of reports related to hydroplaning, runway and tire testing are freely available on the NASA Technical Reports Server (NTRS).

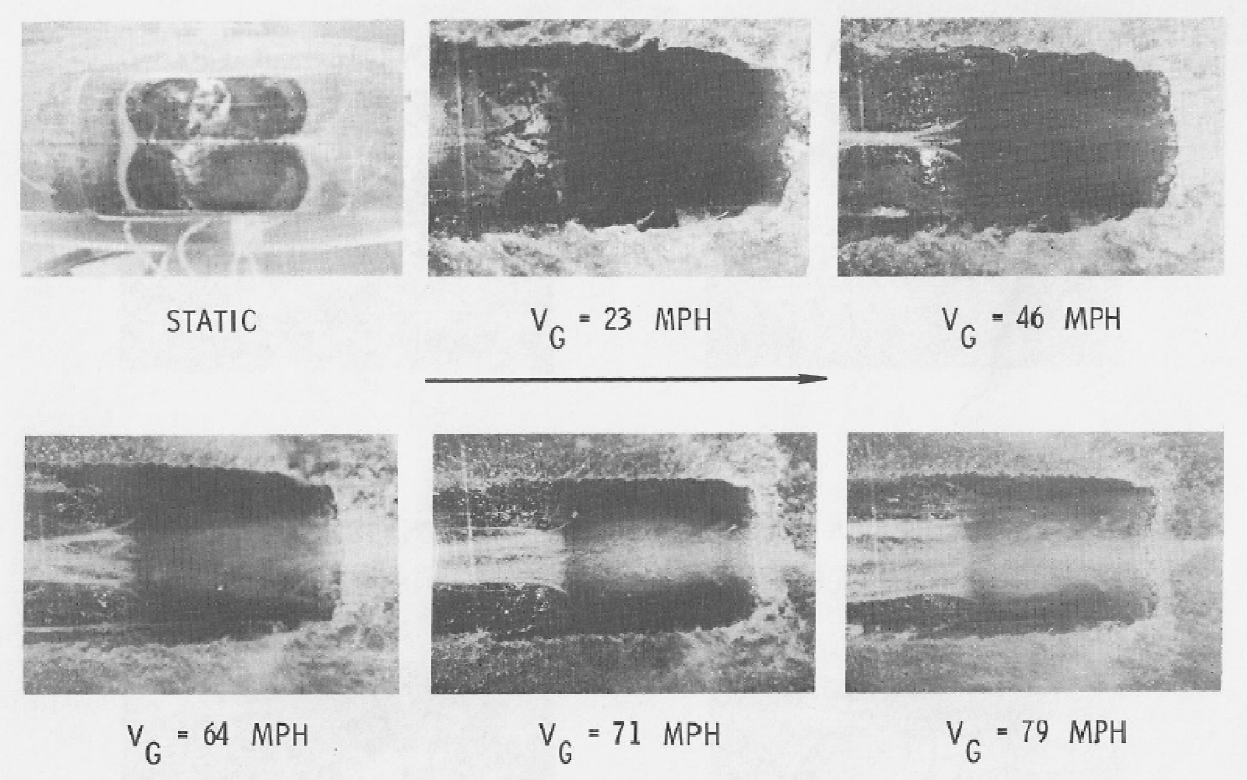

Figure 1. A 6.50-13 Smooth Tread Tire Hydroplaning Above a Glass Plate. Vertical Load = 835 lb_f, Tire Pressure = 27 psi. Reproduced from Figure 2, Horne and Joyner, 1965 [3].

Northwestern University and General Motors Corporation

In the early 1970s, Alan L. Browne completed his PhD dissertation "Dynamic Hydroplaning of Pneumatic Tires" at Northwestern University and continued this research with General Motors Corporation [4]. Brown completed both experimental and theoretical work related to hydroplaning phenomena.

He setup a laboratory experiment with water flow between two aluminum plates that were milled to specific shapes based on the water flow geometry and water film thicknesses beneath a standard smooth tire as reported in several NASA publications. Data on page 8, as well as Figure 2, Figure 19 and Figure 20 from Horne and Joyner's 1965 paper were used in the development of Browne's experiment [3]. He also sought film thickness data from Figure 21 in Horne and Dreher's 1963 report and from Williams' 1968 report [1], [5]. The schematic of the milled aluminum plate is shown in Figure 2. The numbers shown within the plate are height values equivalent to the difference between one inch and the water film thickness Browne determined from the aforementioned NASA publications.

Browne's experimental work highlights the turbulent nature of the flow during hydroplaning. He also developed a mathematical model that closely resembled the results of his experimental work. Browne's study is also significant because researchers from the National University of

Singapore first created finite element models of a hydroplaning tire using the information contained in Figure 2.

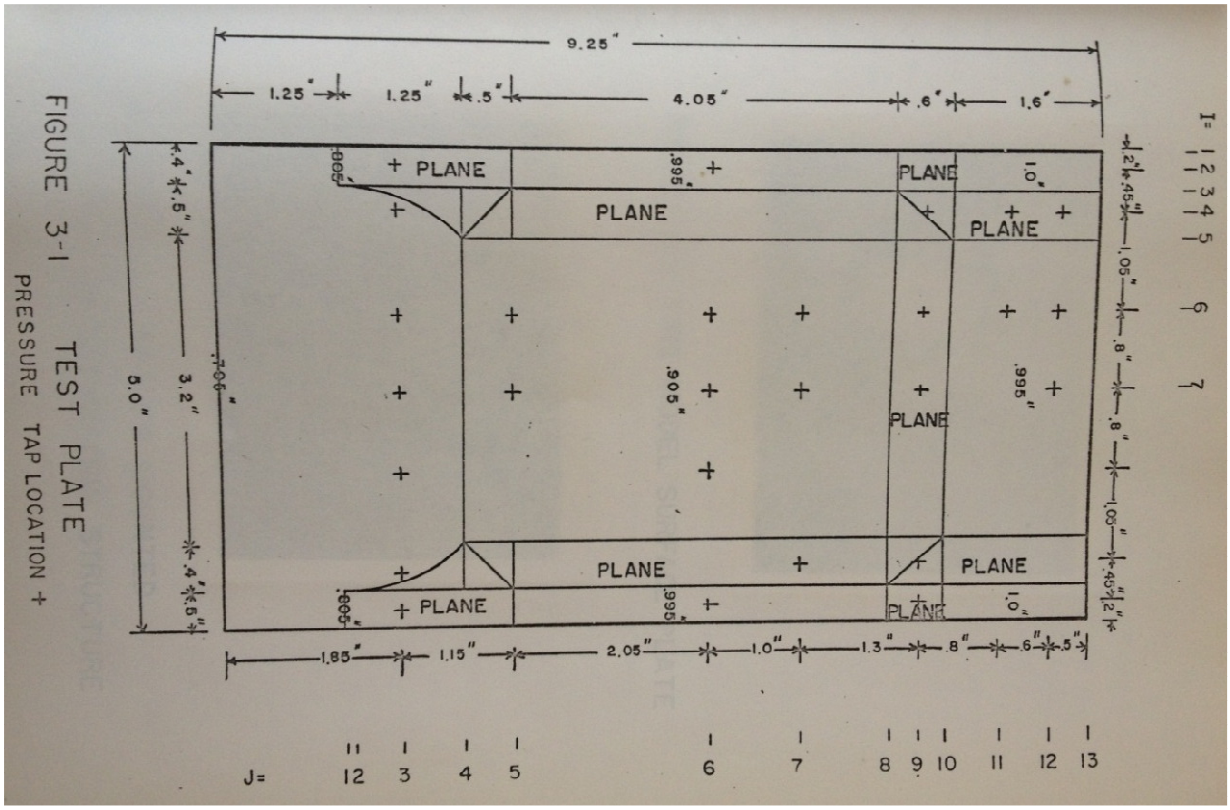

Figure 2. Schematic of Milled Aluminum Plate from Browne's PhD Experiment. Reproduced from Figure 3-1, Browne, 1971 [4].

National University of Singapore

In 2006, G. P. Ong from the Department of Civil and Environmental Engineering at the National University of Singapore completed his doctoral dissertation, "Hydroplaning and Skid Resistance Analysis Using Numerical Modeling" [6]. In this work, Ong developed two and three-dimensional numerical models in an effort to replicate the results of experimental hydroplaning

research conducted previously by several authors, including but not limited to Horne and his colleagues at NASA.

2D CFD Model

Ong begins his dissertation with a thorough literature review and explanation of hydroplaning and wet pavement friction. In section 3.7, he first develops a two-dimensional CFD (computational fluid dynamics) model of the turbulent flow around a geometry based on the fixed deformed tire shape shown in Browne's thesis (Figure 2) which originally comes from three NASA publications [1], [3–6]. This model was developed using the FLUENT CFD software package. The schematic of this model is shown in Figure 3. Using the numerical results of this model, Ong shows that the model does not correlate well to the NASA hydroplaning equation, primarily due to the fact that the lateral pressure outlets beneath the tire cannot be represented without a third dimension.

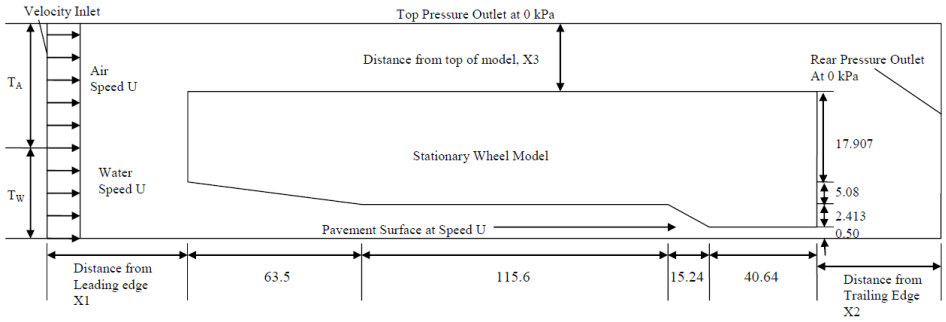

Figure 3. Schematic of Ong's Two-Dimensional CFD Model. Reproduced from Figure 3.6, Ong, 2006 [6].

3D CFD Model

In section 3.8 of his dissertation, Ong develops a three-dimensional CFD model of the turbulent flow around a fixed deformed tire geometry, based on the same figures and values from Browne and NASA [1], [3–6]. This model was developed using the FLUENT CFD software package. The schematic of this model is shown in Figure 4. Since this three-dimensional model incorporated lateral pressure outlets beneath the tire, the numerical results from this model correlated well to the NASA hydroplaning equation. However, since this model's geometry was developed from a specific deformed tire shape, and without access to the glass plate facility and other apparatus used by NASA, this three-dimensional model could not easily be applied to other tires under other load, pressure, velocity and WFT (water film thickness) conditions. Furthermore, since the fixed tire geometry represented the shape of a tire while in the hydroplaning condition, this three-dimensional model could not be used to predict incipient hydroplaning (the conditions required to initiate hydroplaning). Thus, additional modeling work was necessary.

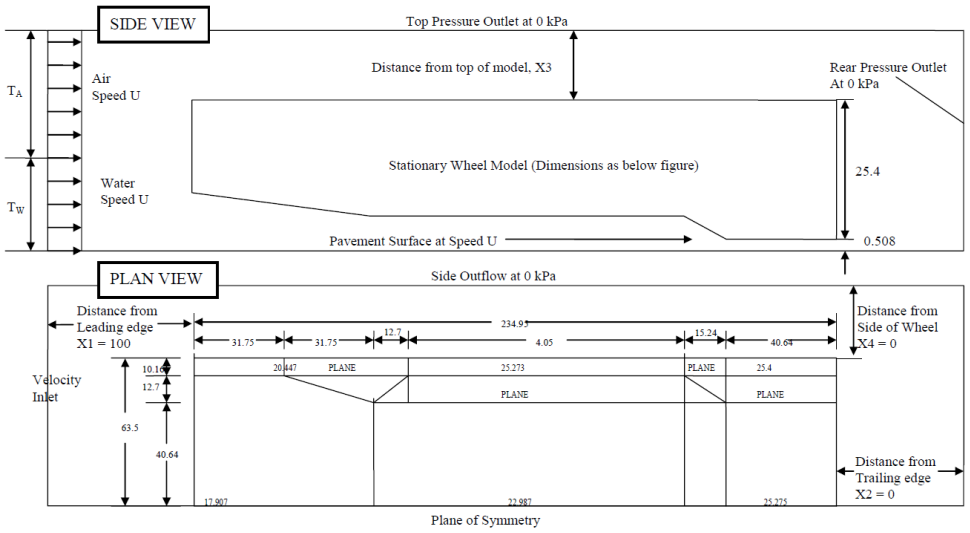

Figure 4. Schematic of Ong's Three-Dimensional CFD Model. Reproduced from Figure 3.5, Ong, 2006 [6].

3D FSI Model

In chapter 7 of his dissertation, Ong develops a three-dimensional FSI (fluid-structure interation) model of a hydroplaning tire [6]. This model was developed using the ADINA FEM software package. This FSI model incorporates two FEM (finite element method) sub-models: a pneumatic tire and pavement surface structural FEM model as shown in Figure 5 and a turbulent CFD fluid model as shown in Figure 6.

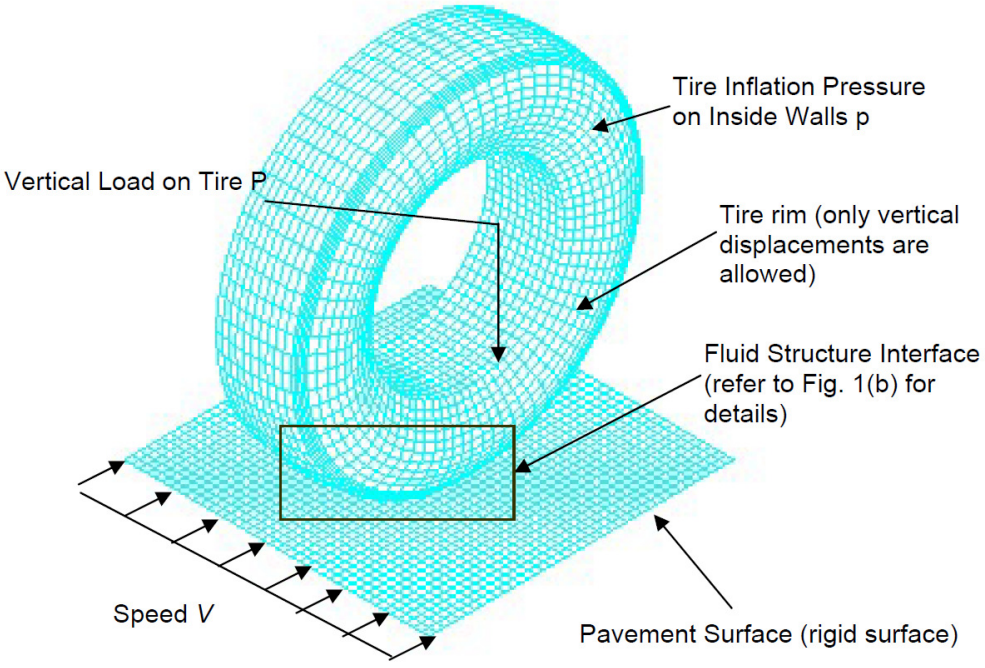

Figure 5. Ong's Pneumatic Tire Sub-Model. Reproduced from Figure 7.1a, Ong, 2006 [6].

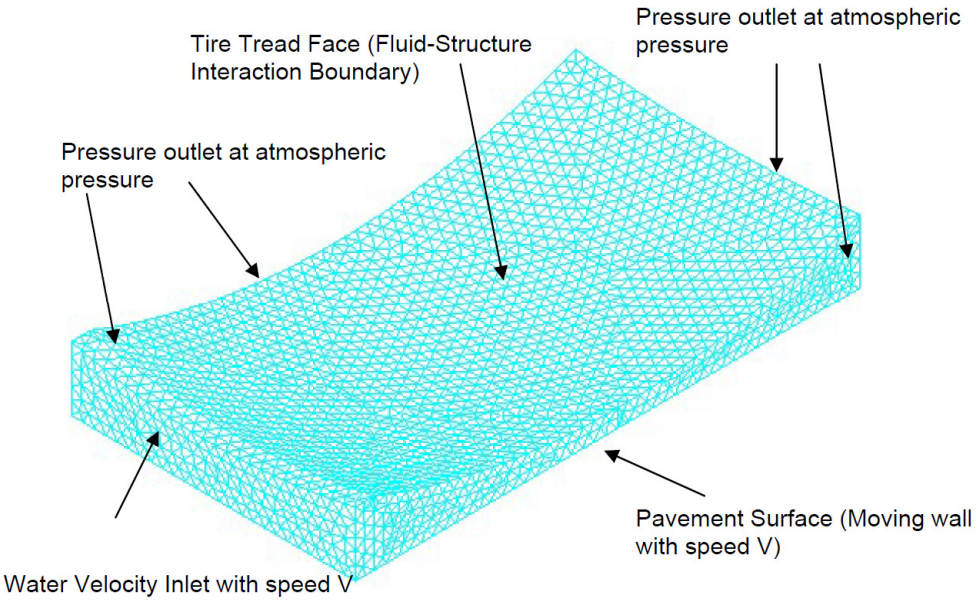

Figure 6. Ong's Fluid Sub-Model. Reproduced from Figure 7.1b, Ong, 2006 [6].

As shown in section 7.2.2. of Ong's dissertation, the pneumatic tire sub-model is composed of three parts: the tire rim, sidewalls and tread [6]. Material properties for these parts are provided as listed in Table 1, yet the exact geometry is not specified. Neither is an explanation provided as to how each of the three parts fit in to the overall geometry. The tire is merely referenced as the ASTM E 524 Standard Smooth Tire. Some discussion is provided as to how the author validated the tire by measuring the FAR (footprint aspect ratio) and comparing it to data provided by a PIARC study from 1995 [7]. The precise procedure within the ADINA software for measuring the FAR is not discussed. However, the outcome of this procedure determined the modulus of elasticity of the tire tread. The tire model is built using 4-node MITC4 (Mixed-Interpolation-of-Tensorial-Components) shell elements. The converged tire model had 5100 shell elements.

Table 1. Structural Components of the Standard Smooth Tire and Their Properties.

Component	Elastic Modulus (GPa)	Poisson's Ratio	Density (kg/m^3)
Rim	100	0.3	2700
Sidewalls	0.02	0.45	1200
Tread	0.1	0.45	1200

As shown in section 7.2.5 of Ong's dissertation, the Navier-Stokes equations and the k-ε turbulence model are used to model the fluid flow within the fluid sub-model [6]. Although a description of the geometry is not available, fluid material properties and turbulence model constants are provided. The density and dynamic viscosity of the fluid (water) were prescribed to be 997.1 kg/m^3 and $0.894 \cdot 10^{-3}$ N·s/m^3 respectively. The k-ε turbulence model coefficients were prescribed as $C_1 = 1.44$, $C_2 = 1.92$, $C_3 = 0.8$, $C_\mu = 0.09$, $\sigma_k = 1$, $\sigma_\varepsilon = 1.3$, and $\sigma_t = 0.9$. The fluid boundary conditions were prescribed as shown in Figure 6. A total of 18,995 four-node tetrahedral elements are used in the converged mesh.

As shown in section 7.2.6 of Ong's dissertation, fluid-structure interaction (FSI) coupling is used to allow the solid and fluid sub-models to interact. The stress and displacement convergence tolerances are both prescribed to be 0.1%, while ε_0, a stress and displacement override constant which cannot be changed within the Adina graphical user interface (AUI), is set to 10^{-8} (which is the default value).

3D FSI Model for Friction Number Determination

Similar to the 3D FSI model developed in chapter 7 of Ong's dissertation, a 3D FSI model capable of predicting friction number (FN), or what Ong refers to as skid number (SN), for the ASTM E 524 standard smooth tire on impermeable surfaces is developed and demonstrated in chapter 8 [6]. Aside from the introduction of the static coefficient of friction, μ, which is made equivalent to FN at 0 mph (shown as FN_0), the model variables are identical to those values pertaining to the 3D FSI model from Ong's chapter 7. In section 8.5.1, Ong shows that FN at a given speed can be determined from the fluid uplift and fluid drag forces imparted to the tire at the given speed. One form of Ong's equations 8.3 and 8.4 are shown below, where FN_v is the friction number at a given speed v, F_x is the total horizontal force imparted to the tire, F_z is the total vertical load imparted to the tire, $F_{traction}$ is the component of F_x contributed by the pavement, F_{drag} is the component of F_x contributed by the fluid, μ is the coefficient of friction, F_{uplift} is the vertical fluid force imparted to the tire, and F_{drag} is the horizontal fluid force imparted to the tire.

$$FN_v = \frac{F_x}{F_z} * 100 = \left(\frac{F_{traction} + F_{drag}}{F_z}\right) * 100 = \left(\frac{\mu\left(F_z - F_{uplift}\right) + F_{drag}}{F_z}\right) * 100$$

Ong validates his model with hydroplaning data from several sources including Rose and Gallaway (1977) [8], Horne (1969) [9], Horne and Tanner (1969) [10], and Agrawal and Henry (1977) [11]. In section 8.3.1 of his dissertation, Ong describes the back-calculation process used to determine the FN_0 for his model curves that correspond to the data he uses for validation. The comparison of the results of Ong's simulation and the experimental data from Rose and Gallaway, Horne, Horne and Tanner and Agrawal and Henry are shown in Figure 7, Figure 8, and Figure 9.

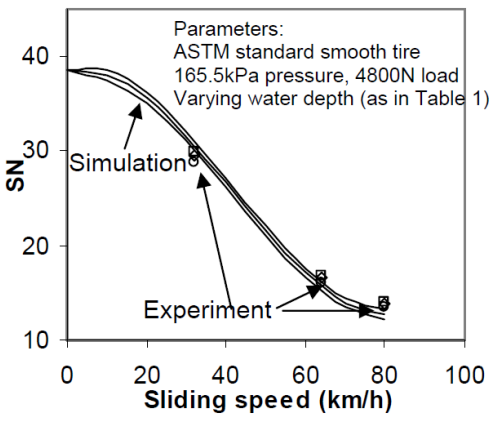

(a) Concrete (Rose and Gallaway 1977)

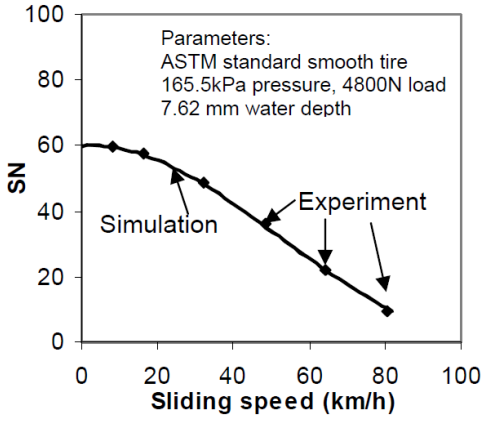

(b) Ungrooved concrete (Horne 1969)

Figure 7. Comparison of Ong's Simulation Results with Experimental Data from Rose and Gallaway and Horne. Reproduced from Figure 8.1, Ong, 2006 [6].

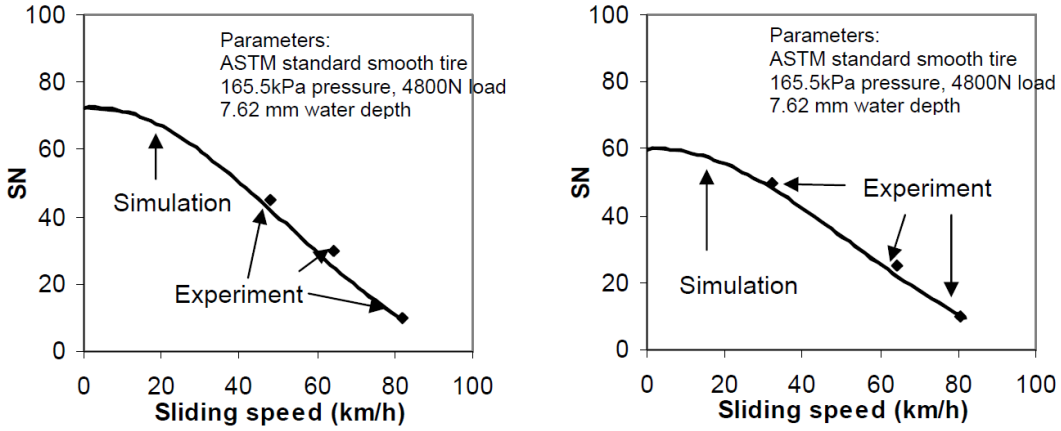

(c) Asphalt (Horne 1969) (d) Concrete (Horne and Tanner 1969)

Figure 8. Comparison of Ong's Simulation Results with Experimental Data from Horne and Horne and Tanner. Reproduced from Figure 8.1, Ong, 2006 [6].

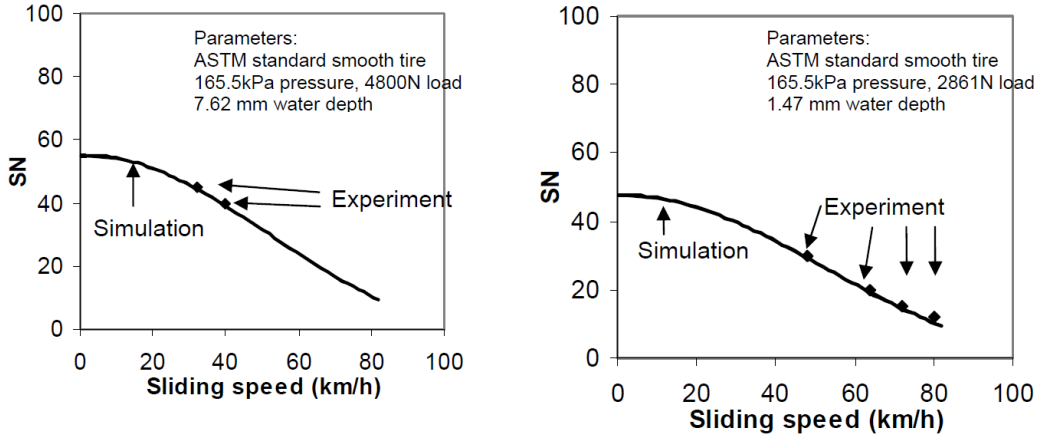

(f) Small-aggregate asphalt(Horne and Tanner 1969) (h) Smooth concrete (Agrawal and Henry 1977)

Figure 9. Comparison of Ong's Simulation Results with Experimental Data from Horne and Tanner and Agrawal and Henry. Reproduced from Figure 8.1, Ong, 2006 [6].

3D FINITE ELEMENT MODEL DEVELOPMENT

The 3D finite element model developed herein was largely based on the work of G. P. Ong and T. F. Fwa from the National University of Singapore (NUS) [6], [12], with some additional support from the work of other advisees of T. F. Fwa [13–15]. The finite element models produced by NUS that were relevant to this study were created using the ADINA software package. Since only general modeling parameters were provided by NUS authors, it was unclear from the outset which specific software settings were employed to produce a working 3D finite element model. Thus, additional assistance was sought from the ADINA software manuals [16–18] and technical support team.

Overall Concept of Model

The 3D finite element model developed herein was designed to emulate the action of the locked-wheel in the skid test described in ASTM E 274. Unlike in the standard skid test, which sprays a jet of water onto the tire, it is assumed that the tire will interact with a certain thickness of water above a planar pavement, known as the water film thickness (WFT). As shown in Figure 10a, a stationary observed would view a locked wheel dragged at speed U along a planar pavement surface into an originally stationary water film. This is mathematically equivalent to the situation depicted in Figure 10b, where a stationary tire is impacted by a water film and a pavement surface moving at speed -U. This scenario, as shown in Figure 10b, is used as the basis for the 3D finite element model.

The specific type of finite element analysis performed with ADINA for this hydroplaning simulation is called fluid-structure interaction (FSI). In ADINA, an FSI analysis requires two model files, an ADINA structures file, and an ADINA computational fluid dynamics (CFD) file. The structures file contained information relevant to the tire and pavement surface, while the CFD file contained information relevant to the water between the tire and pavement.

Structural Modeling

The structures file contains two geometric entities: the tire and the pavement. The tire model is based on the ASTM E 524 standard smooth tire. The schematic shown in ASTM E 524 was scanned, imported into AutoCAD, and traced in AutoCAD. The result is shown in Figure 11. Certain tire dimensions are provided in Section 5 and Figure 2 of ASTM E 524 and these were used when appropriate. In section 7.2.2 of his dissertation, Ong states that he used 4-node shell elements for the tire mesh [6]. This is advantageous because a shell-based model can be run in a relatively short amount of time compared to a model built with solid elements that may contain as many as 27 nodes which would take significantly longer to run. Thus, after the ASTM E 524 tire schematic was traced using AutoCAD, a line about the center of the tire wall thickness was drawn in order to aid in the establishment of two-dimensional surfaces in ADINA that would eventually be meshed with 4-node shell elements. The line about the center of the tire wall thickness is shown in Figure 12.

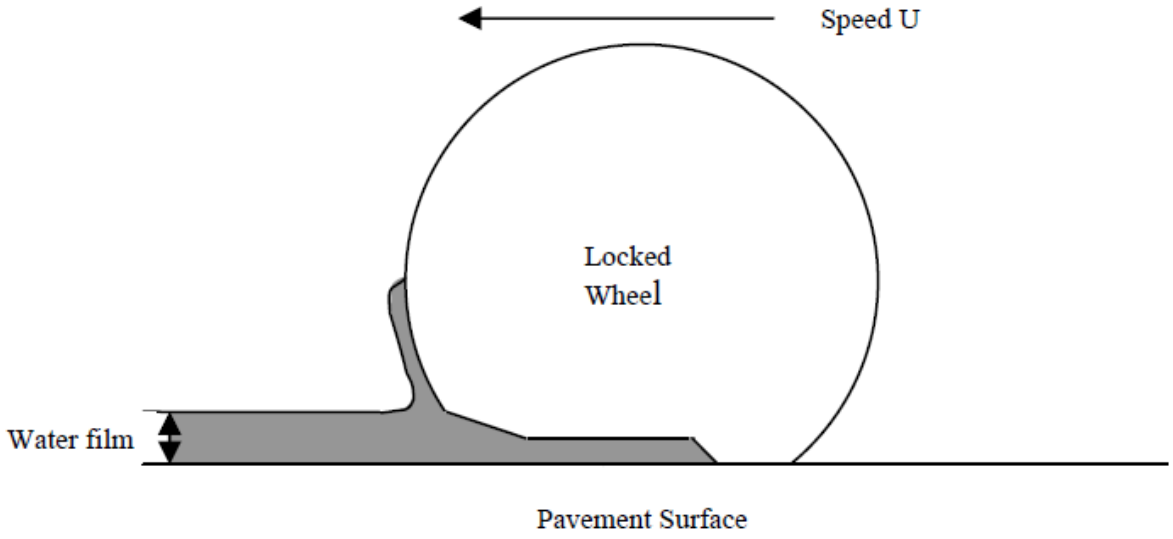

(a) Stationary observer frame of reference

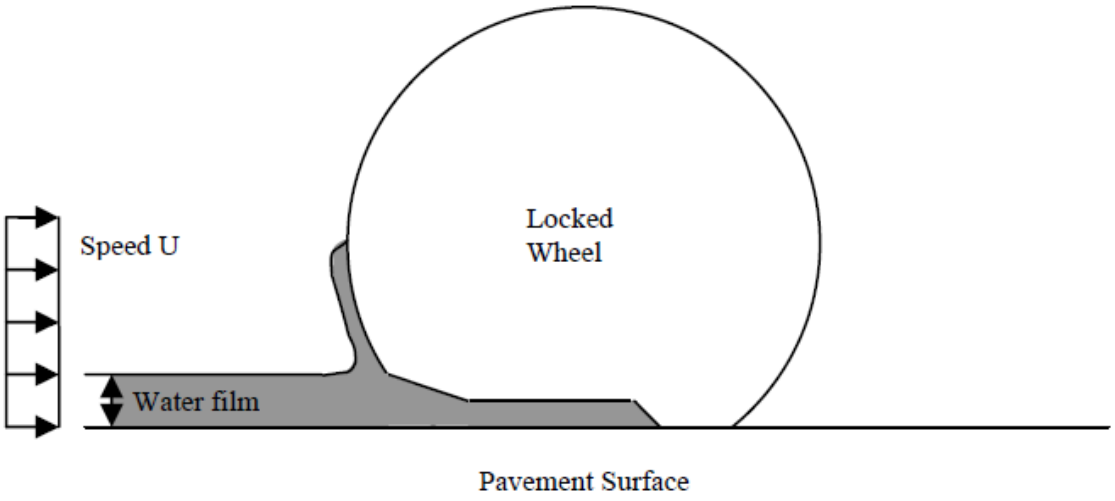

(b) Moving wheel frame of reference

Figure 10. Wheel Frame of Reference. Adapted from Figure 3.2, Ong, 2006 [6].

AutoCAD provided geometric information about the arcs that comprise the center line in Figure 12. This information was inputted into ADINA and the geometry of the tire cross-section is shown in Figure 13. This cross-section was rotated 360 degrees about the y-axis to form surfaces as shown in Figure 14. Per ASTM E 274, the Standard Test Method for Skid Resistance of Paved Surfaces Using a Full-Scale Tire, and ASTM E 524 a total load of 1085 lb_f (4800 N) was applied to the tire rim in the negative z (downward) direction and a tire inflation pressure of

24 psi (165 kPa) was applied to all inner surfaces of the tire in the direction normal to those surfaces. As in section 7.2.2 of Ong's dissertation, three structural components were used to create the tire: the rim, the sidewalls and the tread [6]. Table 1 shows the elastic modulus, Poisson's ratio and density of the three structural components. The tire rim was allowed to move in the z direction, but motion in the x and y directions was disallowed. The tread was assigned the boundary condition of an FSI surface. The tire, meshed with 4-node shell elements, is shown in Figure 15.

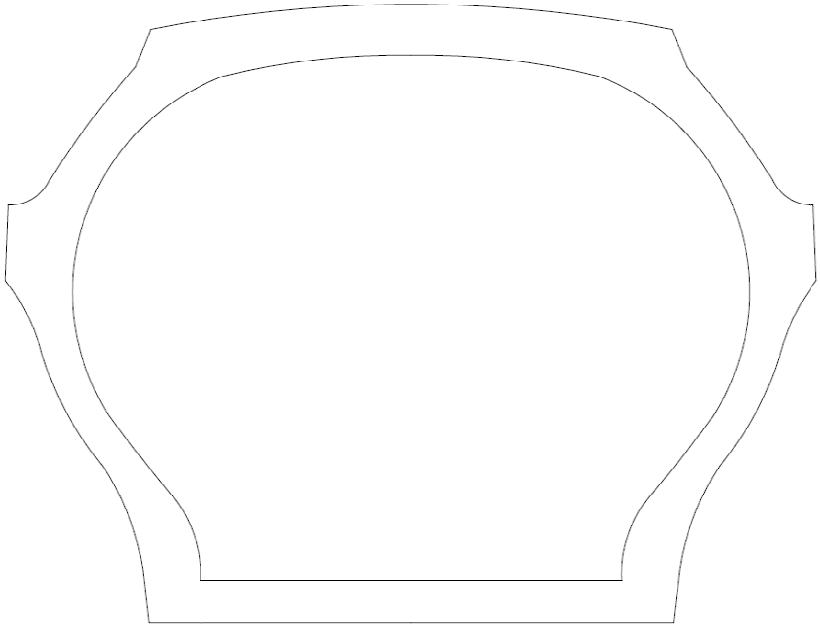

Figure 11. AutoCAD trace of Figure 2 from ASTM E 524 Standard Smooth Tire.

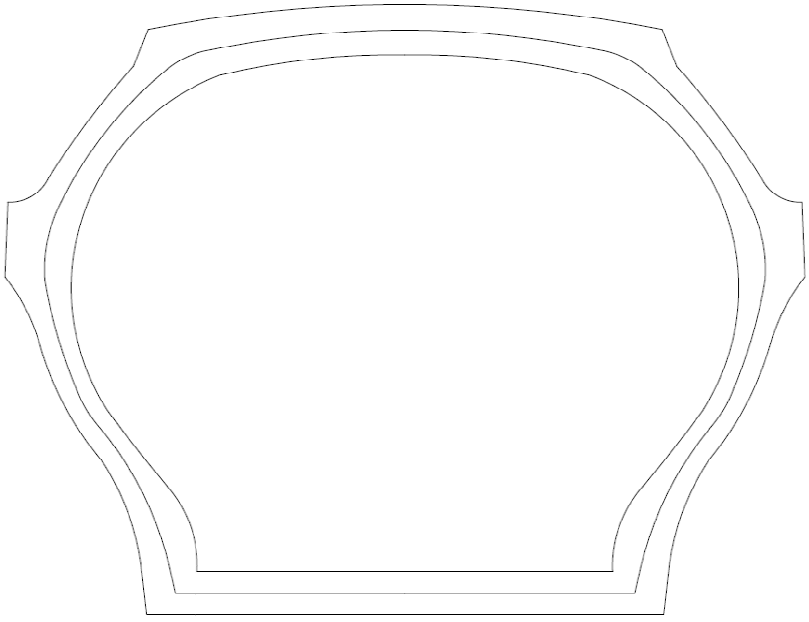

Figure 12. AutoCAD trace of Figure 2 from ASTM E 524 Standard Smooth Tire with center line.

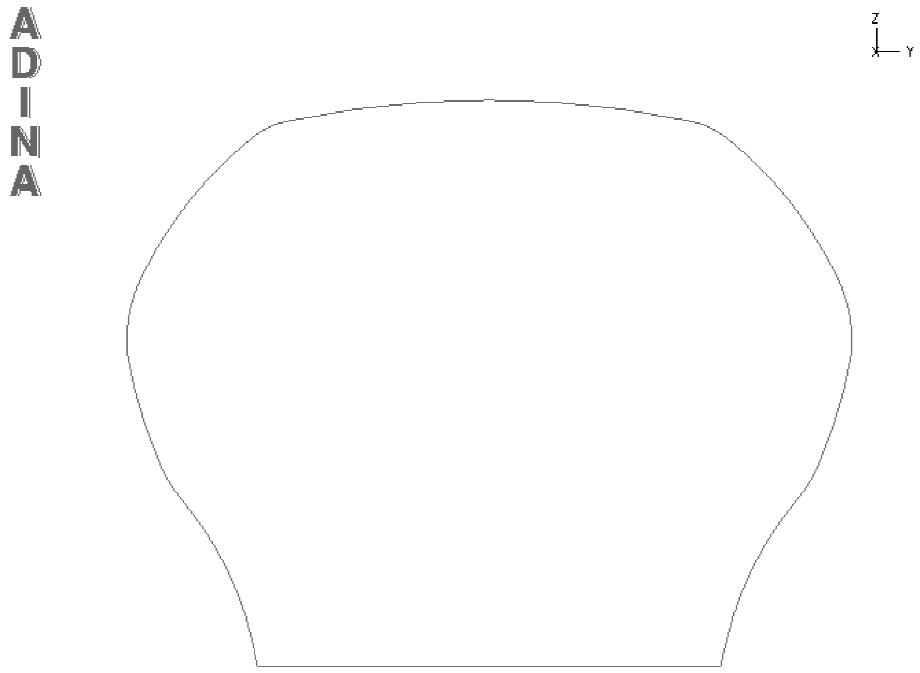

Figure 13. ASTM E 524 Standard Smooth Tire cross section in ADINA.

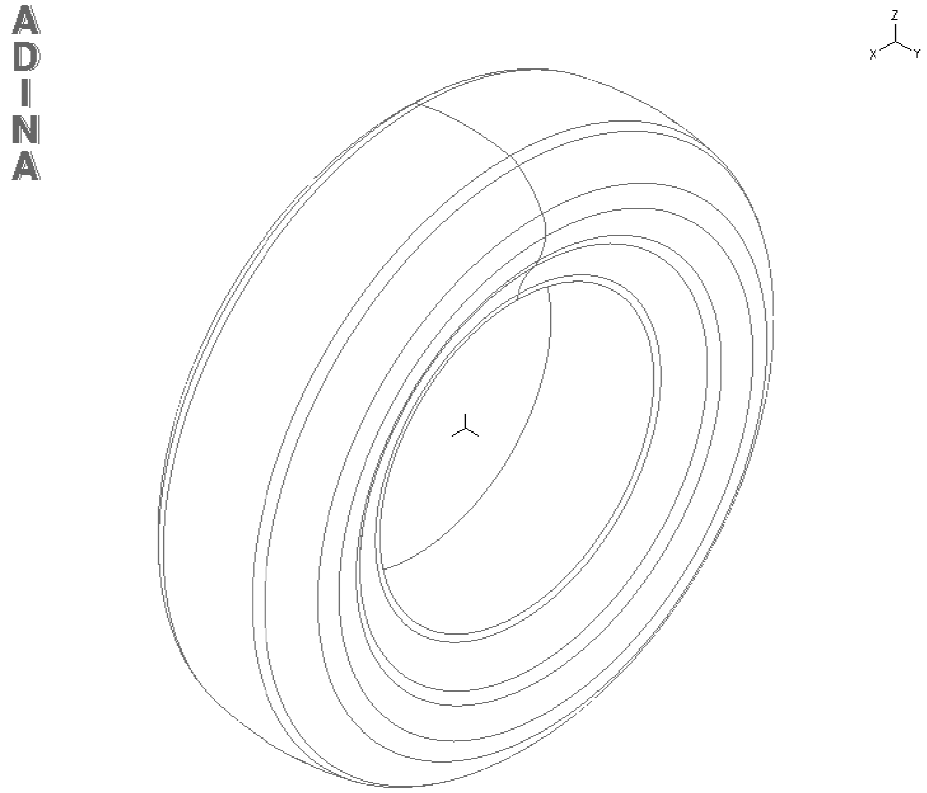

Figure 14. ASTM E 524 Standard Smooth Tire in ADINA.

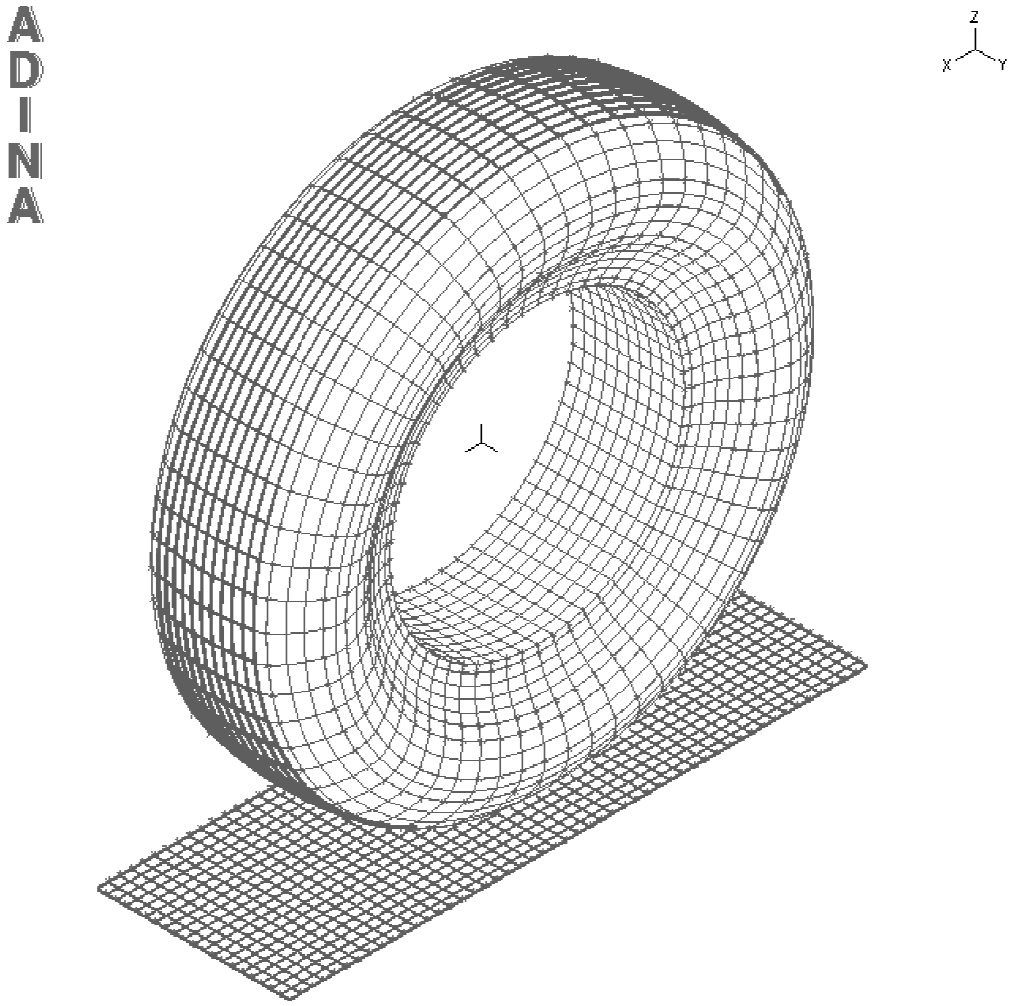

Figure 15. Meshed ASTM E 524 Standard Smooth Tire and Planar Pavement Surface in ADINA.

The pavement surface, as shown in Figure 15, is a rectangular surface that was meshed as a rigid contact surface. Thus, it cannot move and contains no material properties. Similar to section 7.2.4 of Ong's dissertation, contact analysis was setup to allow the tire tread to interact with the planar pavement surface [6].

Fluid Modeling

The fluid geometry is based primarily on the shape of the tread of the undeformed ASTM E 524 standard smooth tire. Two regions, in front of and behind the tire, have been added to the fluid geometry in order to let the fluid reach a steady flow at a semi-infinite distance away from the tire. The fluid boundary conditions are shown in Figure 16.

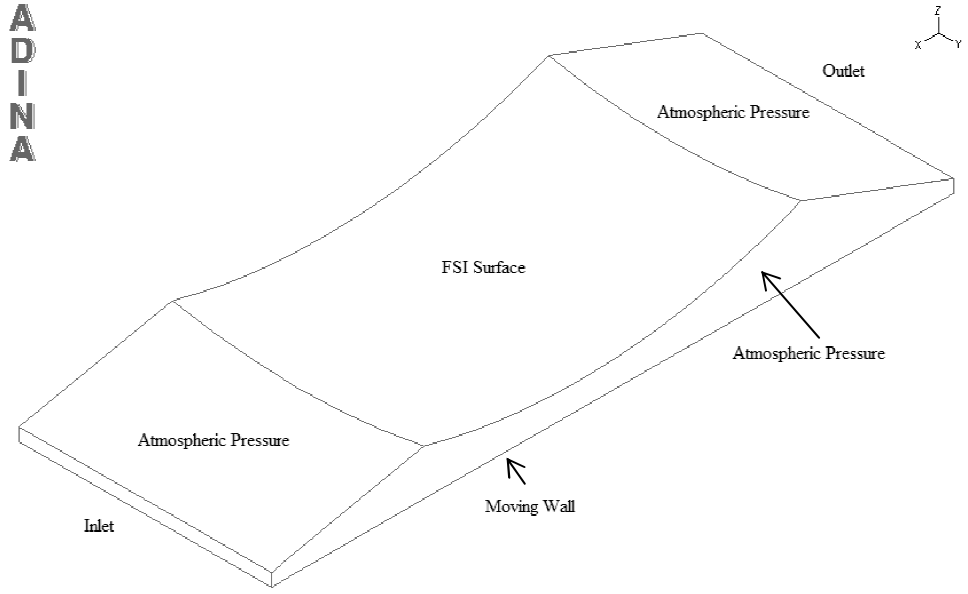

Figure 16. Fluid Geometry with Boundary Conditions.

As in section 7.2.5 of Ong's dissertation, the density and dynamic viscosity of the fluid (water) were prescribed to be 997.1 kg/m^3 and $0.894 \cdot 10^{-3}$ N·s/m^3 respectively. The Navier-Stokes equations are used to model the fluid behavior. As shown in Ong's dissertation and in Wallace's hydroplaning study from 1964, the fluid flow in hydroplaning is largely turbulent [6], [19]. The k-ε turbulence model was used, with coefficients prescribed as $C_1 = 1.44$, $C_2 = 1.92$, $C_3 = 0.8$, $C_\mu = 0.09$, $\sigma_k = 1$, $\sigma_\varepsilon = 1.3$, and $\sigma_t = 0.9$. The desired velocity was assigned to the inlet and to the moving wall. A mapped mesh composed of 8-node brick elements was used for the fluid mesh as shown in Figure 17.

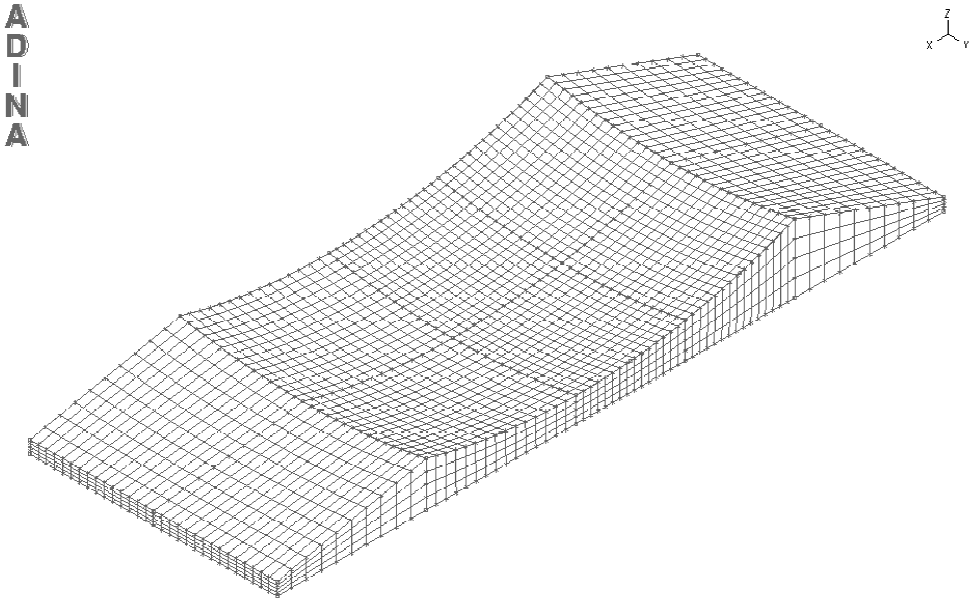

Figure 17. Fluid Mesh in ADINA.

EMPIRICAL FN-SPEED MODEL DEVELOPMENT

In the tables and figures section of chapter 8 of Ong's thesis, he presents his Figure 8.2a, which depicts the FN (referred to as "SN" by Ong) contribution from the fluid drag and the contribution from the tire-pavement contact [6]. This is shown in Figure 18.

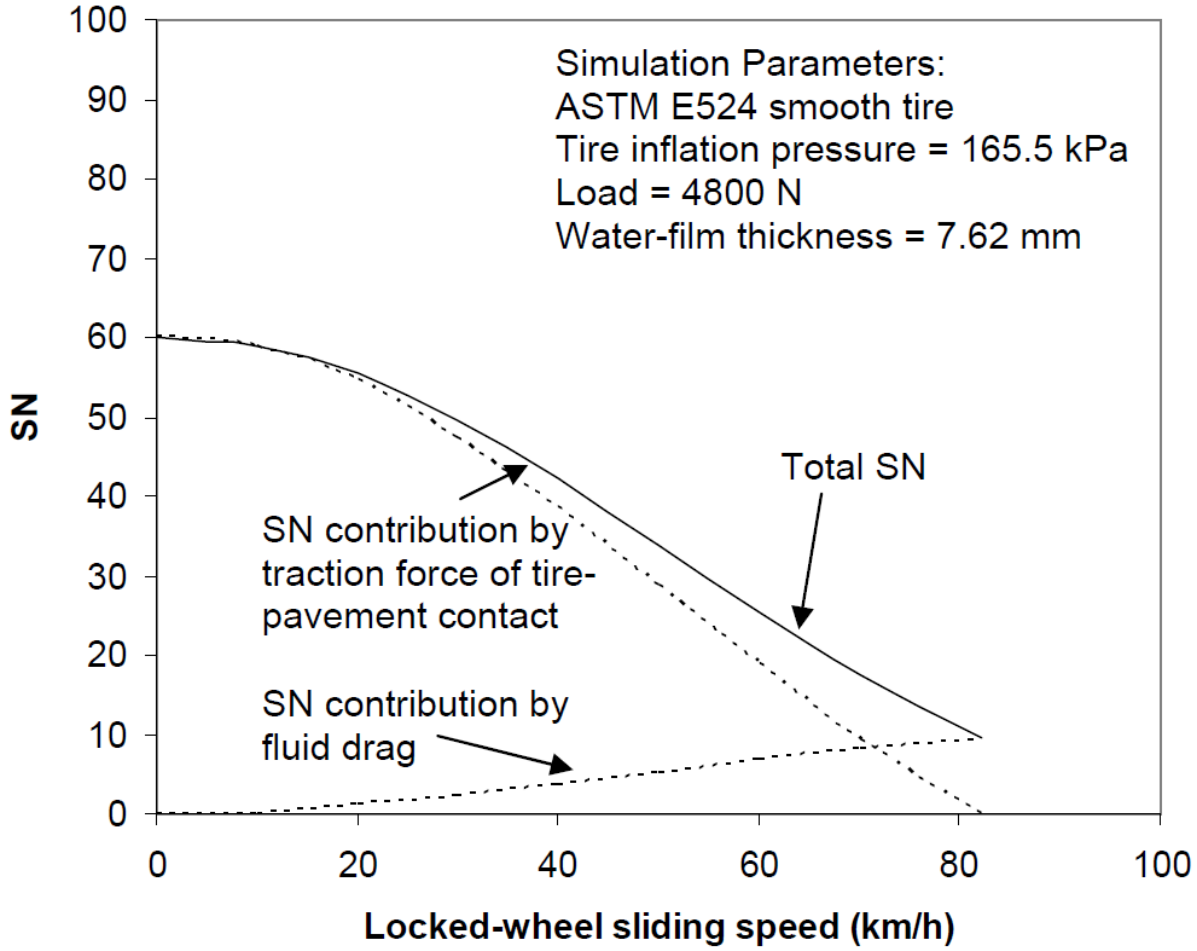

Figure 18. Friction Number and the Contributions from Fluid Drag and Tire-Pavement Contact. Reproduced from Figure 8.2a, Ong, 2006 [6].

The total friction number is also depicted in Figure 18. After carefully extracting data points along the total friction number curve, the friction number vs. speed curve was compared to the simulation and experimental results originally shown in Figure 7, Figure 8 and Figure 9. The comparison is shown in Figure 19, Figure 20 and Figure 21. In order to make the comparison, the friction number values extracted from Figure 18 were multiplied by the ratio of the FN_0 value pertaining to the given curve in Figure 7, Figure 8 or Figure 9 (reported in Ong's table 8.2) to 60, the FN_0 for the total friction number curve shown in Figure 18. After this procedure was complete, it showed that the general shape of the FN-speed curve in Figure 18 was a near perfect fit for charts b-h in Figure 7, Figure 8 and Figure 9 and a reasonable fit for chart a in Figure 7. Since all of the surfaces listed in Figure 7, Figure 8 and Figure 9 are impermeable, it supports the

observation that friction number as a function of speed is primarily dependent upon the friction number at 0 mph.

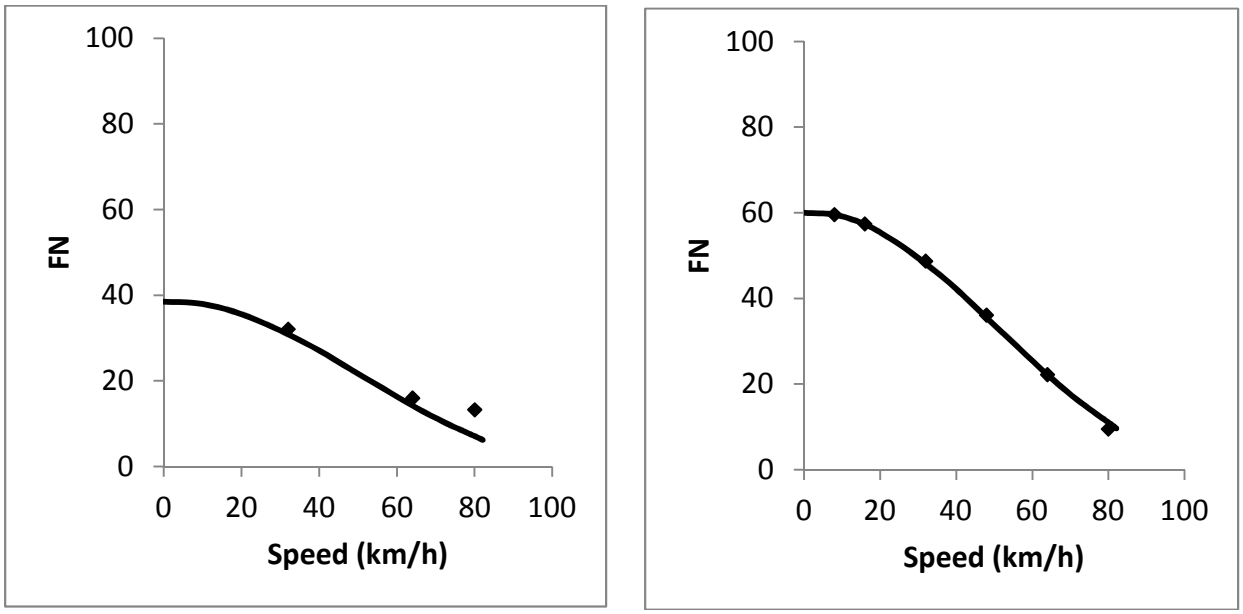

Figure 19. Recreation of Figure 7 using the Total FN Curve from Figure 18.

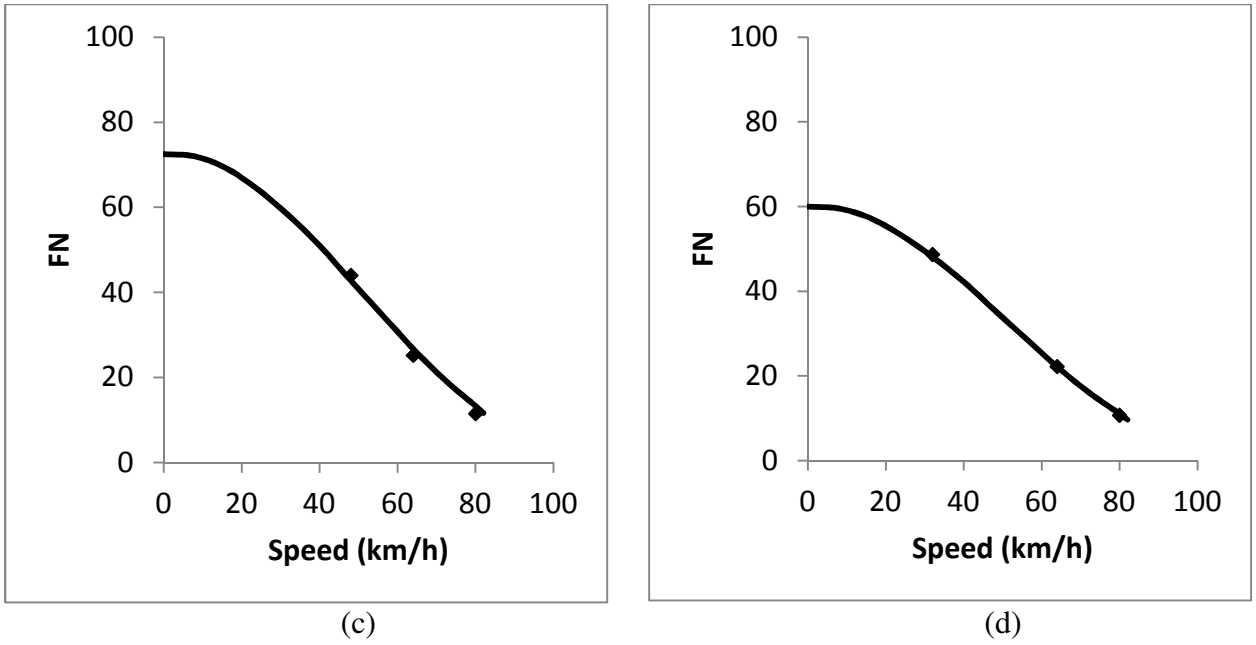

Figure 20. Recreation of Figure 8 using the Total FN Curve from Figure 18.

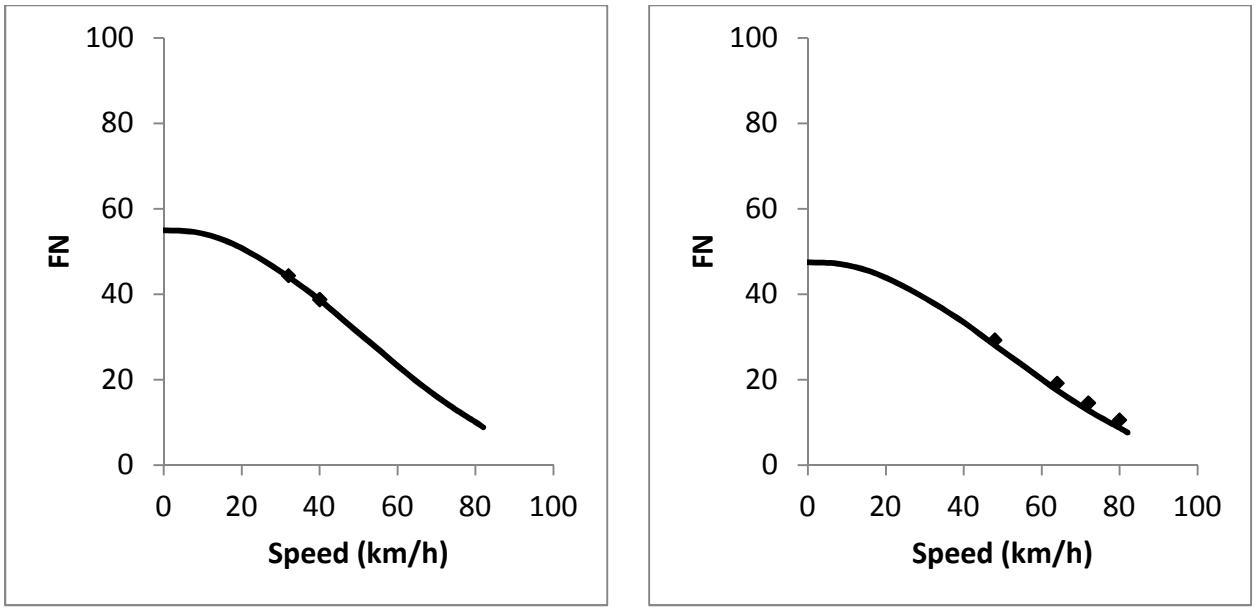

(e) (f)

Figure 21. Recreation of Figure 9 using the Total FN Curve from Figure 18.

In 2012, Zhang, Ong and Fwa from the National University of Singapore published a paper at the TRB annual meeting that demonstrates a 3D FSI model capable of predicting the friction number at a given speed for permeable surfaces [20]. The experimental data by which Zhang et al. validated their model came from a study published by Younger in 1994 [21], [22]. It was desired to match the total FN curve from Figure 18 to the data published by Younger and reported by Zhang et al. In order to do this, the total FN curve was shifted based on testing a variety of values of FN_0 and C_V, a velocity shift constant. The shifted total FN curve provides an excellent match to the data published by Younger, as shown in Figure 22.

The process of applying a shifted version of the total FN curve from Figure 18 (also referred to as a "hydroplaning curve") to experimental data can also be applied to two FDOT studies: "Harmonization of Texture and Skid Resistance Measurements" by Jackson et al., 2008 [23] and "Harmonization of Texture and Friction Measurements on Florida's Open and Dense Graded Pavements" by Choubane et al., 2012 [24]. Figure 23 shows the hydroplaning curves matched to the data from the dense graded sites from Jackson et al., 2008. Figure 24 shows the hydroplaning curves matched to the data from the open graded sites from Jackson et al., 2008. Figure 25 shows the hydroplaning curves matched to the data from the dense graded sites from Choubane et al., 2012. Figure 26 shows the hydroplaning curves matched to the data from the open graded sites from Choubane et al., 2012.

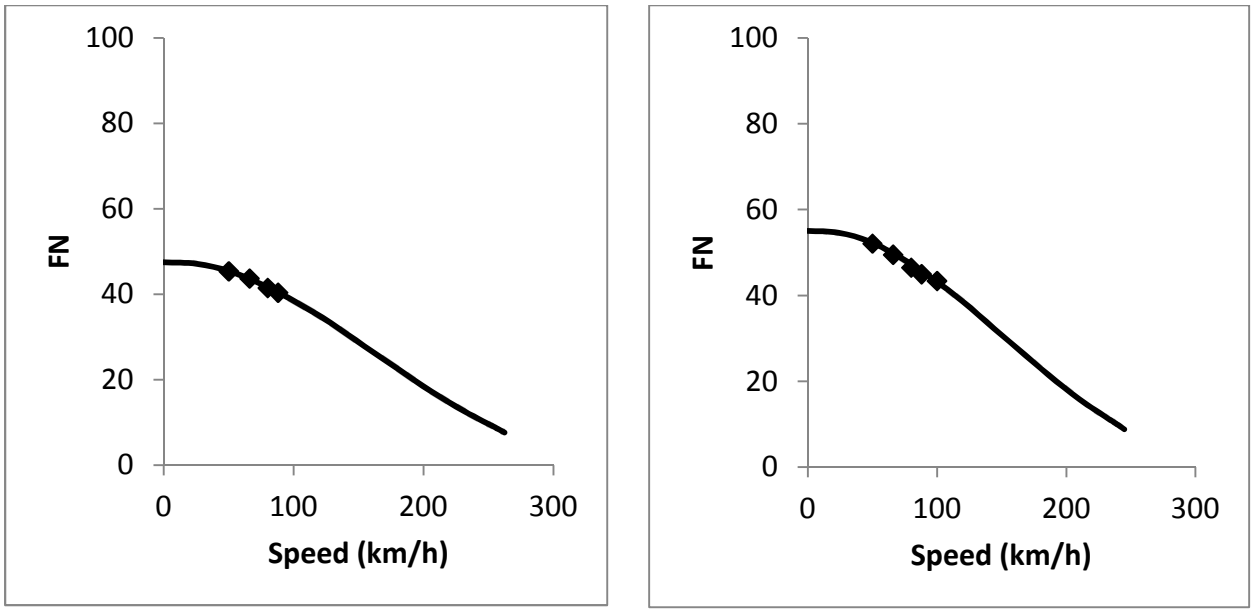

Figure 22. Total FN Curve from Figure 18 Matched to Data from Younger, 1994 [21], [22] shown in Zhang, 2012 [20]. Left: Data for 50 mm Porous Layer Thickness. Right: Data for 100 mm Porous Layer Thickness.

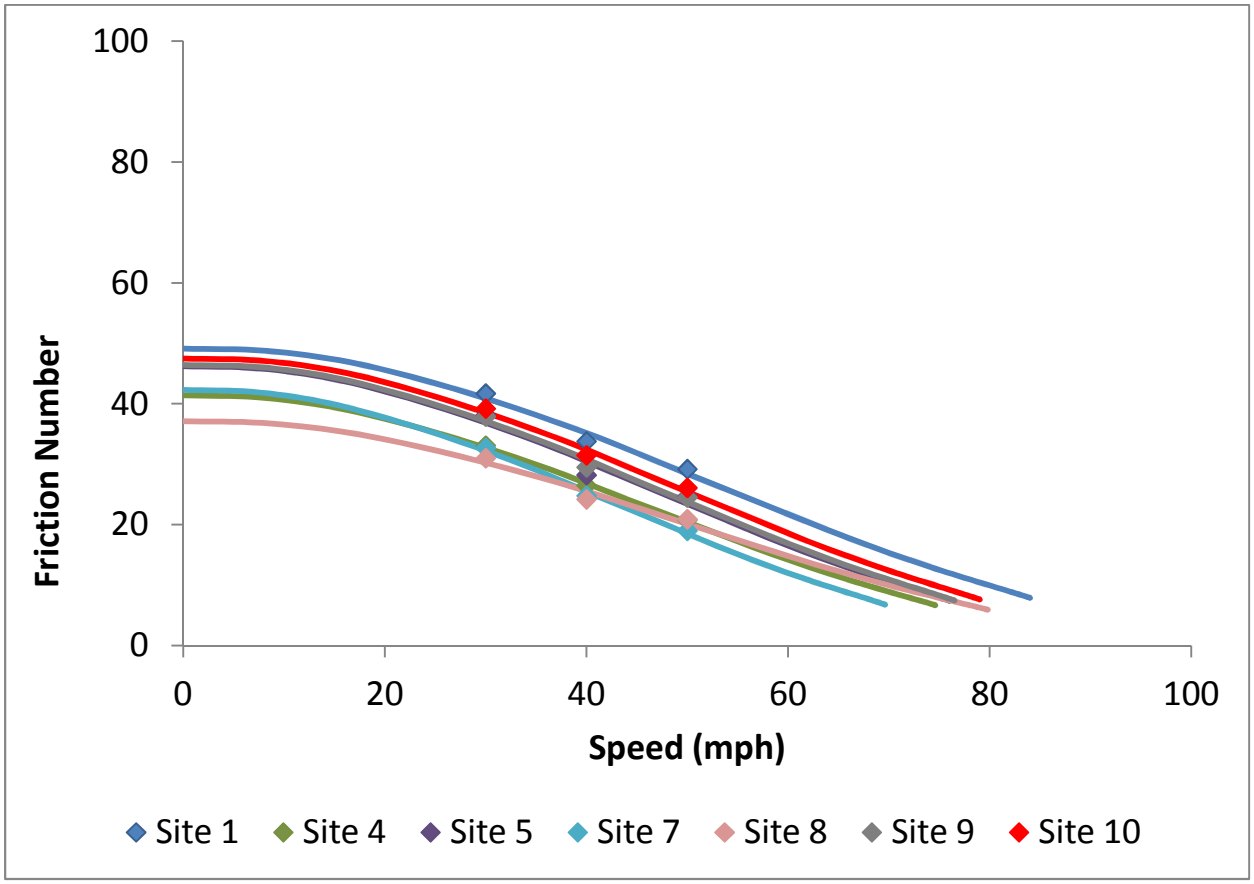

Figure 23. Hydroplaning Curves Matched to the Data from Dense Graded Sites from Jackson et al., 2008 [23].

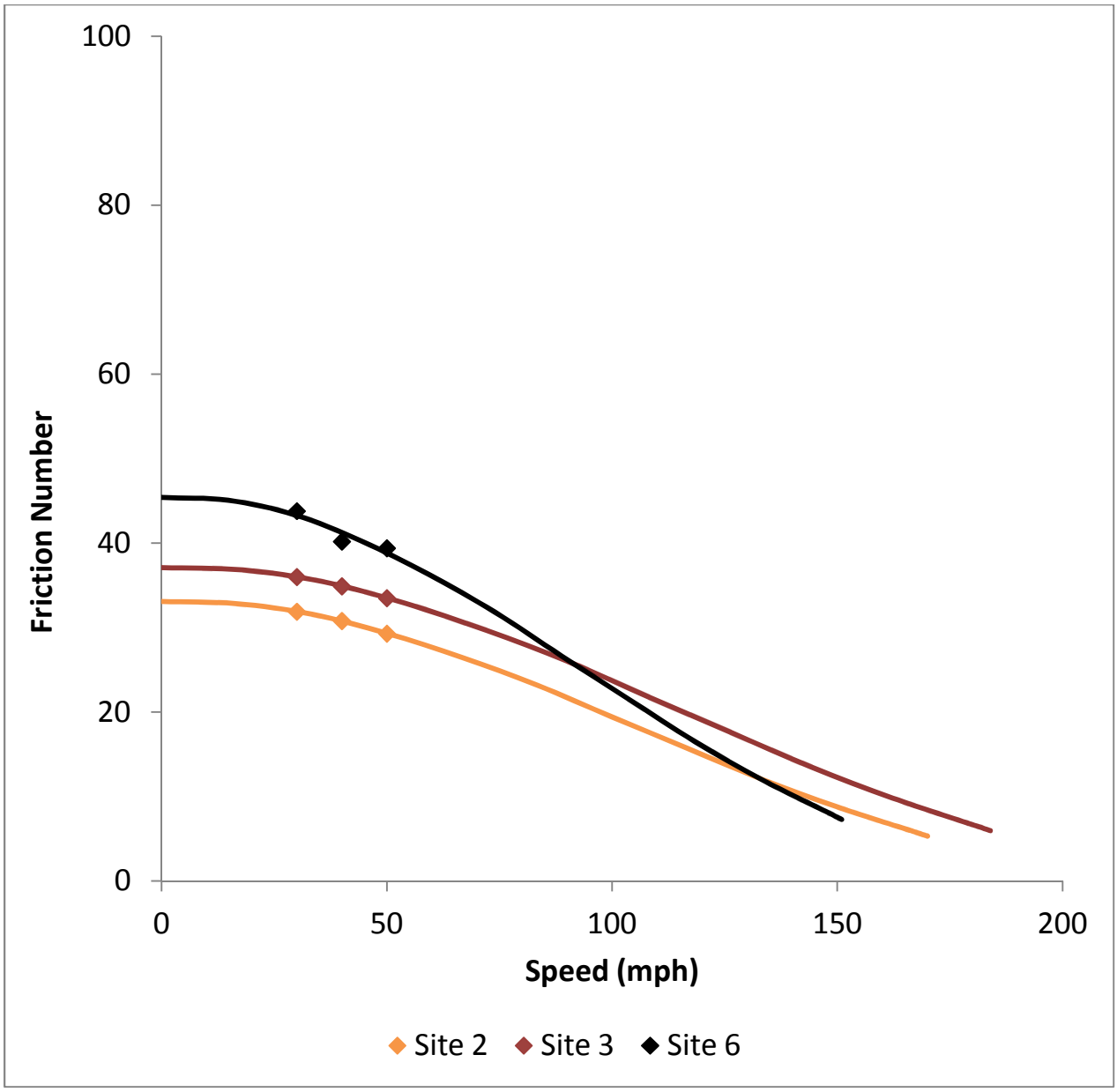

Figure 24. Hydroplaning Curves Matched to the Data from Open Graded Sites from Jackson et al., 2008 [23].

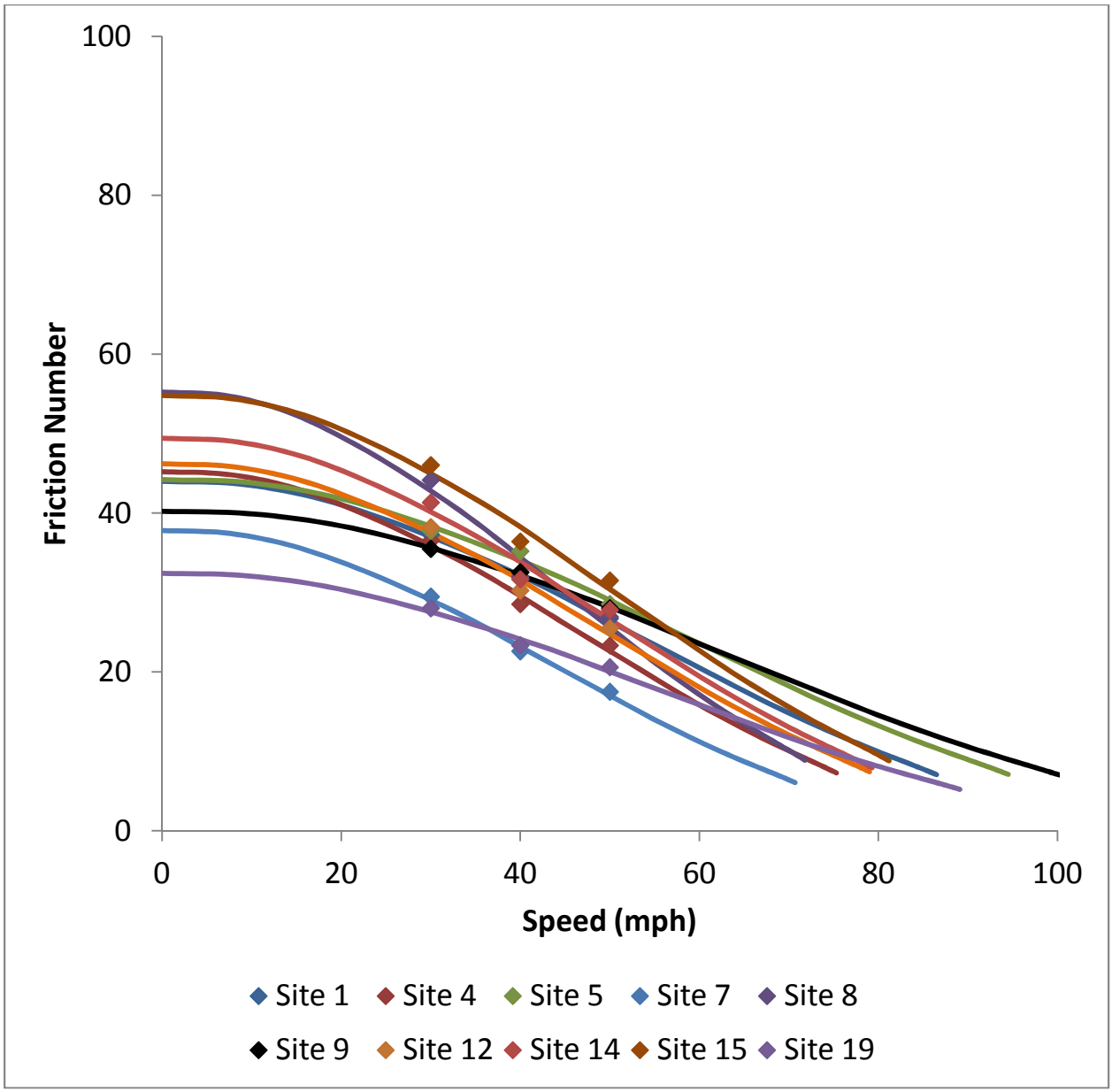

Figure 25. Hydroplaning Curves Matched to the Data from Dense Graded Sites from Choubane et al., 2012 [24].

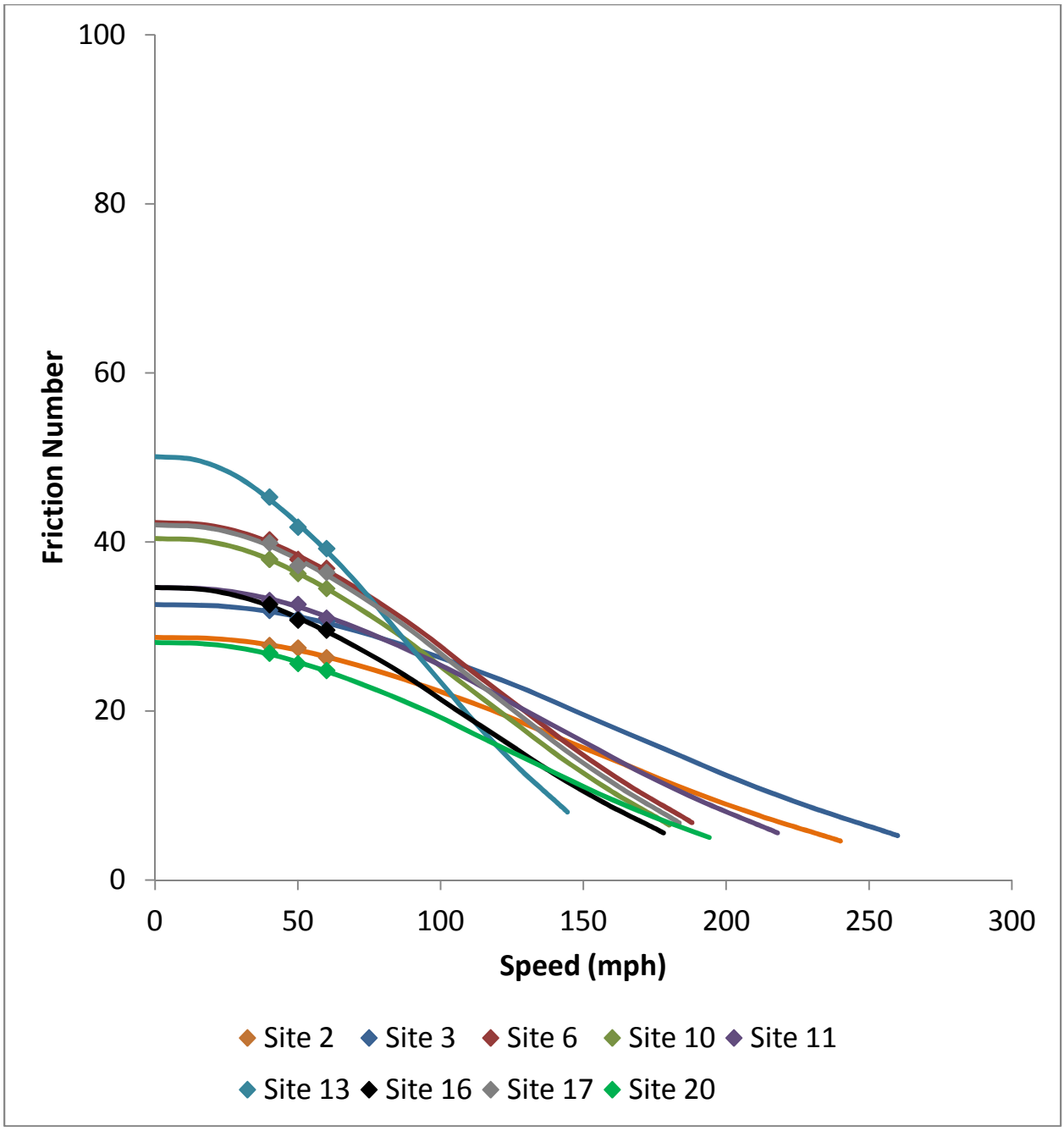

Figure 26. Hydroplaning Curves Matched to the Data from Open Graded Sites from Choubane et al., 2012 [24].

Although the hydroplaning curve is shifted by adjusting FN_0 and C_V, relevant measurements taken in the field are FN_{40} (which can be correlated to FN_0) and MPD (which can be correlated to C_V). It was determined that the relationship between FN_0 and FN_{40} varies with surface type, whereas the relationship between C_V and MPD varies with aggregate. Both of these relationships are linear, as shown in the following equations:

$$FN_0 = A * FN_{40} + B$$

$$C_V = C * MPD + D$$

The constants A, B, C and D are show in Table 2 and Table 3.

Table 2. Surface Type Contants.

Surface	A	B
FC 5	1.1849	-4.2059
FC 9.5	1.2534	9.4052
FC 12.5	1.1851	9.3561

Table 3. Aggregate Constants.

Aggregate	C	D
Granite	1732.6	45.077
Limestone	3528.6	10.751

In order to create a hydroplaning curve for a given pavement, it must have a surface type of FC 5, FC 9.5 or FC 12.5 and be composed of either granite or limestone. Gather the MPD depth value in inches, and the value of FN_{40} (where 40 is in mph). Using the appropriate constants from Table 2 and Table 3, plug in the value of FN_{40} and MPD in order to determine FN_0 and C_V. Using Table 4, multiply each value of speed by the ratio $C_V/51$ and multiply each value of FN by the ratio $FN_0/60$ in order to determine the values of speed and friction number that, when plotted, show the specific hydroplaning curve.

Table 4. Default Values of Speed and Friction Number.

Speed (mph)	FN
0	60.000
5	59.554
10	57.274
15	53.167
20	47.994
25	42.059
30	35.211
35	28.514
40	21.818
45	15.883
50	10.710
51	9.645

An example of this process follows. For site 3 in Jackson, 2008, the pavement was FC 5 Granite, with FN_{40} = 34.9 and MPD = 0.0754 inches [23]. Using Table 2 and Table 3, constants A, B, C and D are 1.1849, -4.2059, 1732.6, and 45.077 respectively. Using the equations for FN_0 and C_V shown above, FN_0 = 1.1849 * 34.9 – 4.2059 = 37.147 and C_V = 1732.6 * 0.0754 + 45.077 = 175.72. Using the ratio of $C_V/51$ = 3.4455 and the ratio of $FN_0/60$ = 0.61912 and multiplying by

the values of speed and FN, respectively, in Table 4, new values of speed and FN are generated as shown in Table 5.

Table 5. Values of Speed and FN for Site 3 from Jackson, 2008 [23].

Speed (mph)	FN
0.00	37.147
17.23	36.871
34.46	35.460
51.68	32.917
68.91	29.714
86.14	26.040
103.37	21.800
120.59	17.654
137.82	13.508
155.05	9.834
172.28	6.631
175.72	5.971

A plot of the values shown in Table 5, including the original value of FN40 and boundary lines at FN = 10 and Speed = 80 mph is shown in Figure 27.

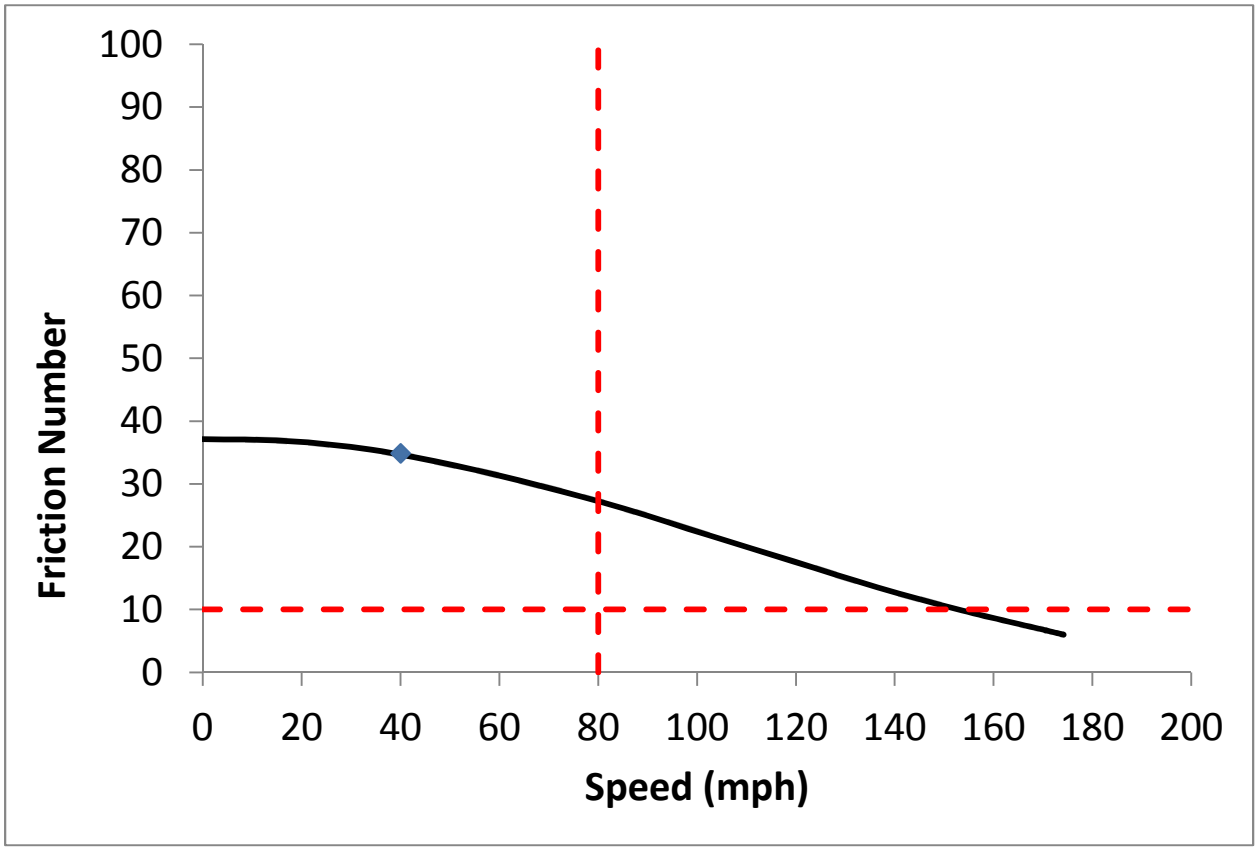

Figure 27. Hydroplaning Curve for Site 3 from Jackson, 2008 [23].

In the case of site 3 from Jackson, 2008, the hydroplaning curve is an excellent fit based on the value of FN_{40} and MPD provided. Not all values of FN_{40} and MPD for a given pavement will produce a curve where the value of FN_{40} is found directly along the curve, yet the hydroplaning curve will still show a general trend that highlights whether the predicted friction number at 80 mph is acceptable (above 10) or is not acceptable (below 10). It is noted that in this example, the pavement surface is an open-graded friction course, and thus the potential for hydroplaning at typical highway speeds is extremely low.

CONCLUSIONS

The objective of this research was to develop a methodology for the reliable prediction of hydroplaning speed for specific pavement design surfaces and materials employed on Florida roadways. The research consisted of an extensive literature review and modeling of hydroplaning conditions on typical FDOT roadway sections. The resulting mechanistic/empirical model is based on pavement condition inputs as obtained from field surveys currently performed by FDOT. The proposed prediction tool is provided in a MS Excel format for ease of use, and has been presented to the FDOT for further evaluation and practical implementation.

REFERENCES

[1] W. B. Horne and R. C. Dreher, "Phenomena of Pneumatic Tire Hydroplaning," NASA Langley Research Center, Washington, D.C., NASA TN D-2056, 1963.

[2] W. B. Horne and T. J. W. Leland, "Influence of Tire Tread Pattern and Runway Surface Condition on Braking Friction and Rolling Resistance of a Modern Aircraft Tire," NASA, Washington, D.C., TN D-1376, 1962.

[3] W. B. Horne and U. T. Joyner, "Pneumatic Tire Hydroplaning and Some Effects on Vehicle Performance," in *International Automotive Engineering Congress*, 1965.

[4] A. L. Browne, "Dynamic Hydroplaning of Pneumatic Tires," Northwestern University, 1971.

[5] J. R. Williams, "Aquaplaning - The British Ministry of Technology Programme," NASA, SP-5073, 1968.

[6] G. P. Ong, "Hydroplaning and Skid Resistance Analysis Using Numerical Modeling," National University of Singapore, 2006.

[7] J. C. Wambold, C. E. Antle, J. J. Henry, and Z. Rado, "International PIARC Experiment to Compare and Harmonize Texture and Skid Resistance Measurements," PIARC Technical Committee on Surface Characteristics, 1995.

[8] J. G. Rose and B. M. Gallaway, "Water Depth Influence of Pavement Friction," *ASCE Journal of Transportation Engineering*, vol. 103, no. 4, pp. 491–506, 1977.

[9] W. B. Horne, "Results from Studies of Highway Grooving and Texturing at NASA Wallops Station," NASA, Washington, D.C., SP-5073, 1969.

[10] W. B. Horne and J. A. Tanner, "Joint NASA - British Ministry of Technology Skid Correlation Study - Results from American Vehicles," 1969.

[11] S. K. Agrawal and J. J. Henry, "Technique for Evaluating Hydroplaning Potential of Pavements," *Transportation Research Record No. 633*, pp. 1–7, 1977.

[12] G. P. Ong and T. F. Fwa, "Prediction of Wet-Pavement Skid Resistance and Hydroplaning Potential," *Transportation Research Record No. 2005*, pp. 160–171, 2007.

[13] C. Y. Cao, "Skid Resistance and Hydroplaning Analysis of Rib Truck Tires," National University of Singapore, 2010.

[14] K. Anupam, "Numerical Simulation of Vehicle Hydroplaning and Skid Resistance on Grooved Pavement," National University of Singapore, 2012.

[15] H. R. Pasindu, "Incorporating Risk Considerations in Airport Runway Pavement Maintenance Management," National University of Singapore, 2011.

[16] "ADINA Primer," ADINA R & D, Inc., ARD 11-7, 2011.

[17] "ADINA Theory and Modeling Guide, Volume I: ADINA Solids & Structures," ADINA R & D, Inc., ARD 11-8, 2011.

[18] "ADINA Theory and Modeling Guide, Volume III: ADINA CFD & FSI," ADINA R & D, Inc., ARD 11-10, 2011.

[19] K. B. Wallace, "Airfield Pavement Skidding Characteristics," Melbourne, Australia, 1964.

[20] L. Zhang, G. P. Ong, and T. F. Fwa, "Developing an Analysis Framework to Quantify and Compare Skid Resistance Performances on Porous and Non-Porous Pavements," in *92nd Transportation Research Board Annual Meeting*, 2012.

[21] K. D. Younger, "Evaluation of Porous Pavements Used in Oregon," Oregon State University, 1994.

[22] K. D. Younger, R. G. Hicks, and J. Gower, "Evaluation of Porous Pavements Used in Oregon," Oregon Department of Transportation, SPR 5298, 1994.

[23] N. M. Jackson, C. Holzschuher, and B. Choubane, "Harmonization of Texture and Skid Resistance Measurements," Florida Department of Transportation, FL/DOT/SMO/08-BDH-23, 2008.

[24] B. Choubane, H. S. Lee, C. Holzschuher, P. Upshaw, and N. M. Jackson, "Harmonization of Texture and Friction Measurements on Florida's Open and Dense Graded Pavements," *Transportation Research Record No. 2306*, 2012.

APPENDIX

MS Excel Hydroplaning Model Instructions

1) Open the MS Excel sheet entitled “Hydroplaning Empirical Model.xlsx” and dated June 14, 2013

2) Choose “Surface Type” from the drop down menu: FC 5, FC 9.5 or FC 12.5

3) Choose “Aggregate Type” from the drop down menu: Limestone or Granite.

4) Input the appropriate “Friction Number” obtained at 40 mph, and based on the ASTM E 274 using ASTM E 524 Standard Smooth Tire.

5) Input the appropriate “Mean Profile Depth” obtained from the FDOT high speed laser profile measurement, in inches.

6) The graph of predicted Friction Number versus Vehicle Speed (mph) will be automatically displayed.

7) The proper interpretation of the graph is that the potential for hydroplaning is likely at or above speeds where the predicted Friction Number is in the vicinity of 10.